Nanoscale

PAPER

View Article Online
View Journal | View Issue

Cite this: *Nanoscale*, 2023, **15**, 15975

Selective and controlled H_2 generation upon additive-free HCOOH dehydrogenation over a Pd/NCS nanocatalyst†

Qing Zhang,[a] Yanlan Wang,[b] Xiaotao Jin[a] and Xiang Liu *[a]

Received 31st July 2023,
Accepted 6th September 2023

DOI: 10.1039/d3nr03797e

rsc.li/nanoscale

Although sodium formate is widely used as a conventional additive to enhance selective H_2 evolution from HCOOH dehydrogenation, this leads to a waste of resources and an increase in the cost of H_2 production. For this reason, N-doped carbon nanospheres with abundant graphitic C/N have been designed to enrich the electron cloud density of the Pd atom for improving its catalytic activity in H_2 generation upon additive-free HCOOH dehydrogenation. Herein, we have synthesized N-doped carbon nanosphere-stabilized Pd nanoparticles (Pd/NCSs) as high-efficiency nano-catalysts, *via* fixation of Pd nanoparticles onto N-doped carbon nanospheres (NCSs), for selective and controlled H_2 generation upon additive-free HCOOH dehydrogenation. Pd/NCS-800 (1640 h^{-1}) provided a 12 times larger TOF than commercial Pd/C (134 h^{-1}) in H_2 generation upon additive-free HCOOH dehydrogenation. It seemed that graphitic N/C of NCS-800 enriched the electron cloud density of the Pd atom, which was favorable for the cleavage of C–H bonds in HCOOH dehydrogenation. In addition, the selective H_2 evolution from additive-free HCOOH dehydrogenation over Pd/NCS-800 is successfully controlled by adjusting the pH.

[a]*Engineering Research Center of Eco-Environment in Three Gorges Reservoir Region of Ministry of Education, College of Materials and Chemical Engineering, China Three Gorges University, Yichang, Hubei 443002, China. E-mail: xiang.liu@ctgu.edu.cn*

[b]*Department of chemistry and chemical engineering, Liaocheng University, 252059 Liaocheng, China*

†Electronic supplementary information (ESI) available. See DOI: https://doi.org/10.1039/d3nr03797e

Xiang Liu

Xiang Liu received his Ph.D. degree at Université de Rennes 1 in 2017. He is now an associate professor and independent researcher at China Three Gorges University. His research interests are organic synthesis, photocatalysis and functionalization, and engineering of transition-metal nanoparticles or nanoclusters for applications in H_2 evolution and water treatment. He has published more than 120 SCI papers in journals such as Adv. Mater., Nat. Commun., Appl. Catal. B. Environ., iScience, ACS Catal., J. Mater. Chem. A, Chem. Sci., Chem. Eng. J. *and so on.*

Introduction

Humanity's high dependence on traditional fossil fuels has caused the growth of greenhouse gas emission (*e.g.* CO_2 and CH_4),[1–3] which leads to ocean acidification, climatic anomaly, global warming and other environmental deterioration.[4–7] To overcome this issue, it is of high significance to develop renewable energy sources, switching from fossil fuels, for a green future.[8–10] Hydrogen (H_2) is identified as the most promising renewable energy carrier because of its superior energy density and environmentally-friendly economy.[11–15] However, physical storage of H_2 gas suffers from low capacity, high costs and explosibility.[16–20] In this regard, a good deal of hydrogen storage materials, for instance methanol,[21–24] borohydrides,[25,26] silicohydrides,[27] ammonia borane,[28] hydrazine hydrate[29] and formic acid,[30–32] are being intensively developed for H_2 generation.

Since 1978,[33] formic acid (HCOOH), which could be readily obtained from biomass, has been deemed as the most promising liquid hydrogen carrier due to its excellent hydrogen storage capacity (4.4 wt% and 53 g L^{-1}), low toxicity, outstanding stability and safe transportation/storage.[34–40] As a consequence, plenty of heterogeneous and homogeneous catalysts have been explored for selective H_2 evolution from formic acid dehydrogenation (HCOOH → H_2↑ + CO_2↑) and preventing CO release from formic acid dehydration (HCOOH → H_2O + CO↑).[41–47] Among them, PdAg bimetal nanomaterials exhibited

superior catalytic activities in H_2 generation from formic acid dehydrogenation because the alloying of Ag could enrich the electron cloud density of the Pd atom in PdAg, which was in favor of C–H bond cleavage in HCOOH dehydrogenation.[48] Although sodium formate is widely used as an additive to improve selective H_2 evolution upon HCOOH dehydrogenation,[49] this leads to a waste of resources and an increase in the cost of H_2 production.

For this reason, we have designed and synthesized N-doped carbon nanospheres with abundant graphitic C/N for enriching the electron cloud density of the Pd atom in additive-free HCOOH dehydrogenation. Herein, we have synthesized N-doped carbon nanosphere-stabilized Pd nanoparticles (Pd/NCSs) as high-efficiency nano-catalysts, *via* fixation of Pd nanoparticles onto N-doped carbon nanospheres (NCSs), for selective and controlled H_2 generation upon additive-free HCOOH dehydrogenation. Then the kinetic behavior and catalytic activity of Pd/NCSs, mechanistic insight using a tandem reaction, CO_2 capture ability, and "on–off" control for selective and controlled H_2 generation upon additive-free HCOOH dehydrogenation were investigated.

Results and discussion

As described in Scheme 1, NCS-700, NCS-800 and NCS-900 were synthesized by the calcination of melamine, α-D-glucose hydrochar and $NaHCO_3$, with a mass ratio of 1.0 : 1.0 : 1.0, at 700 °C, 800 °C and 900 °C under a N_2 atmosphere for 1 h, respectively.[50] Then Pd/NCS-700, Pd/NCS-800 and Pd/NCS-900 were synthesized by using K_2PdCl_4 and NCSs, followed by $NaBH_4$ reduction, respectively. For studying the structure and morphology of NCS and Pd/NCSs, their SEM images were obtained and are shown in Fig. 1. As illustrated in Fig. S1,† the SEM image shows that the NCS precursor has a uniform spherical structure with a mean size of 0.27 μm (Fig. S2†). After high temperature carbonization, the uniform spherical structure was retained in Pd/NCS-700 (0.23 μm, Fig. 1a, b & S3†), Pd/NCS-800 (0.22 μm, Fig. 1c, d & S4†) and Pd/NCS-900 (0.22 μm, Fig. 1e, f & S5†), and the size of the NCSs reduced as the calcination temperature increased. Then, XRD, FTIR, Raman spectrum and BET analyses were employed to measure the microstructure of Pd/NCS-700, Pd/NCS-800 and Pd/NCS-900. As shown in Fig. 2a, a broad diffraction peak of graphitic C (002) at 2θ = 24° appeared in all of the Pd/NCSs (JCPDS 75-1621).[51] Pd (111) and Pd (200) were also found in Pd/NCSs (JCPDS 87-0638),[52] showing that the PdNPs were immobilized on the surface of NCSs. In the FTIR spectra of

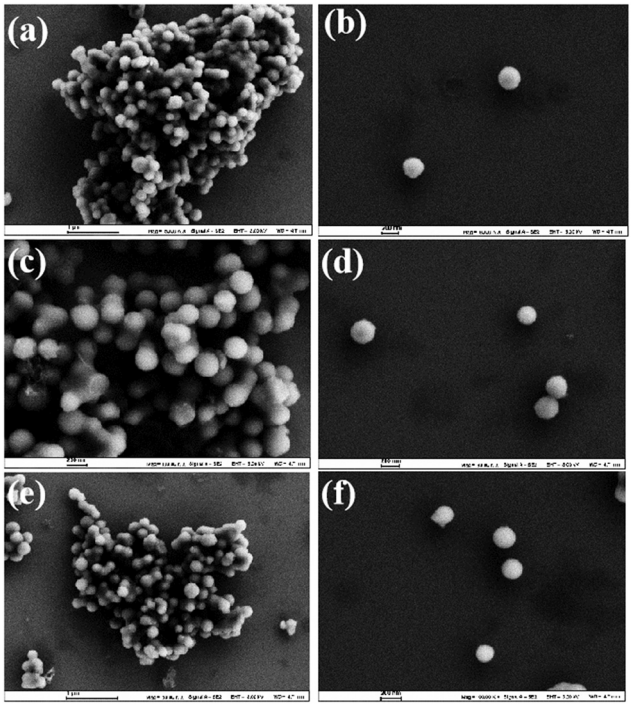

Fig. 1 SEM images of (a and b) Pd/NCS-700, (c and d) Pd/NCS-800 and (e and f) Pd/NCS-900.

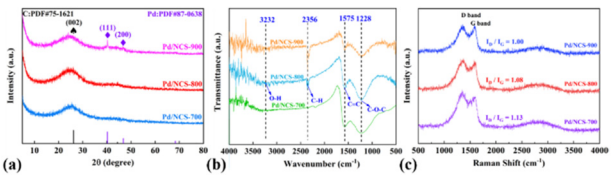

Fig. 2 (a) XRD, (b) FT-IR, and (c) Raman spectra of Pd/NCS-700, Pd/NCS-800 and Pd/NCS-900.

Pd/NCSs (Fig. 2b), the absorption peaks at 3232, 2356, 1575 and 1228 cm^{-1} corresponded to the –OH, C–H, C=C and C–O–C groups, respectively,[53] which were favorable for PdNP stabilization. As presented in Raman spectra (Fig. 2c), the three peaks at 1338, 1613 and 2756 cm^{-1} were assigned to the D-band, G-band and 2D-band, respectively.[54] The values of I_D/I_G in Pd/NCS-700, Pd/NCS-800 and Pd/NCS-900 were 1.00, 1.08 and 1.13, respectively, suggesting that the content of disordered carbon increased as the calcination temperature increased. Moreover, the texture properties of Pd/NCSs were studied by BET analysis. As shown in Fig. S6† and Table 1,

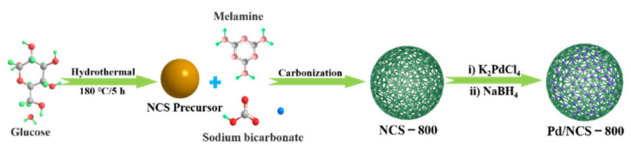

Scheme 1 The synthesis of Pd/NCS-800 nanocomposites.

Table 1 BET analysis of Pd/NCS-700, Pd/NCS-800 and Pd/NCS-900

Catalysts	Surface area ($m^2\ g^{-1}$)	Pore volume ($m^3\ g^{-1}$)	Pore size (nm)
Pd/NCS-700	458.43	0.27	2.34
Pd/NCS-800	572.74	0.33	2.33
Pd/NCS-900	635.09	0.37	2.33

Pd/NCS-900 exhibited a larger surface area and pore volume (635.09 m^2 g^{-1} & 0.37 m^3 g^{-1}) than Pd/NCS-700 and Pd/NCS-800.

First, the catalytic performances of Pd/NCSs in H_2 generation upon additive-free HCOOH dehydrogenation were compared as shown in Fig. S7.† H_2 production was carried out with HCOOH (1 mmol) and 2 mol% of Pd/NCSs in 5 mL of H_2O at 60 °C. It is clear that Pd/NCS-800 exhibited a superior catalytic performance, with a TOF of 1640 h^{-1}, compared to Pd/NCS-700 (1456 h^{-1}) and Pd/NCS-900 (921 h^{-1}) in additive-free HCOOH dehydrogenation. Hence, Pd/NCS-800 was chosen as the optimal catalyst because of its kinetic behavior, recyclability, CO_2 capture ability, tandem reaction, and "on–off" switch of H_2 generation upon additive-free HCOOH dehydrogenation.

For probing why Pd/NCS-800 was so super-efficient in H_2 generation upon additive-free HCOOH dehydrogenation, TEM and HRTEM were employed to confirm the morphology of Pd/NCS-800. From Fig. 3a–e, it is clear that Pd/NCS-800 possessed a homogeneous nanospherical structure, and PdNPs (3.19 nm, Fig. S8†) were successfully stabilized onto the surface of N-doped carbon nanospheres. As shown in Fig. 3f, Pd (111), whose corresponding lattice space is 0.22 nm, was recorded in Pd/NCS-800, verifying the presence of PdNPs on NCSs. Then, the precise localization of Pd, N, O and C elements in Pd/NCS-800 was further investigated by EDX elemental mapping. As described in Fig. 4, the Pd/NCS-800 nanocomposite was made up of palladium, nitrogen, oxygen and carbon elements, verifying that N atoms were successfully doped into carbon nanospheres.

In addition, XPS was employed to investigate the elemental composition and chemical valence of Pd/NCS-800. As displayed in Fig. 5a, the Pd $3d_{5/2}$ spectrum is deconvolved into two peaks of Pd^0 (336.26 eV) and Pd^{II} (337.94 eV), demonstrating that Pd nanoparticles were partly oxidized by air into Pd^{II}.[55] In Fig. 5b, the N 1s spectrum is fitted into four peaks of nitric oxide (405.1 eV, 19.9%), graphitic-N (401.4 eV, 18.5%), pyrrolic-N (399.9 eV, 26.2%) and pyridinic-N (398.2 eV, 35.4%). As displayed in Fig. 5c, the C 1s spectrum is fitted into five typical peaks at 290.3, 288.3, 286.3, 285.4 and 284.6 eV, which are assigned to π–π* (10.05%), C═O (12.49%), C–O (18.58%), C–N (23.28%) and C–C/C═C (35.60%), respectively. As illustrated in Fig. 5d, the O 1s spectrum is fitted into four typical peaks of C–O–C (534.17 eV), C–C═O (532.53 eV), C–OH (531.44 eV) and C═O (530.47 eV), respectively. These results exhibited the presence of N and O-containing functional groups at the Pd/NCS-800 surface. ICP-AES verified that Pd nanoparticles were stabilized onto the surface of NCSs (5.38 wt% Pd, which was slightly smaller than the theoretical value of 6.62 wt%).

The kinetics of H_2 generation upon additive-free HCOOH dehydrogenation (including different Pd/NCS-800 catalyst dosages, various initial HCOOH concentrations and reaction temperatures) was further studied for the potential industrial application. As described in Fig. 6a, the H_2 generation upon additive-free HCOOH dehydrogenation was conducted with various dosages of the Pd/NCS-800 catalyst from 1.5 to 3.0 mol%. The H_2 generation rate elevated as the Pd/NCS-800

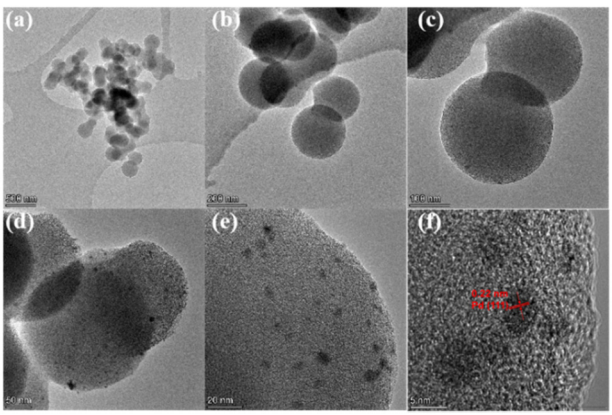

Fig. 3 (a)–(e) TEM and (f) HRTEM images of Pd/NCS-800.

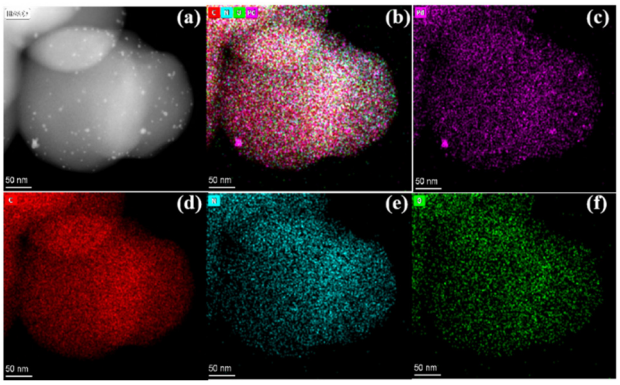

Fig. 4 (a) STEM and (b) combined C, N, O and Pd, (c) Pd, (d) C, (e) N and (f) O EDX mapping of Pd/NCS-800.

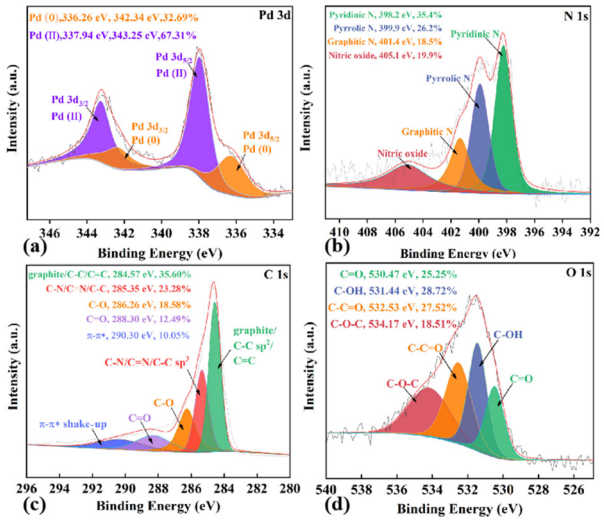

Fig. 5 (a) Pd 3d, (b) N 1s, (c) C 1s and (d) O 1s XPS of Pd/NCS-800.

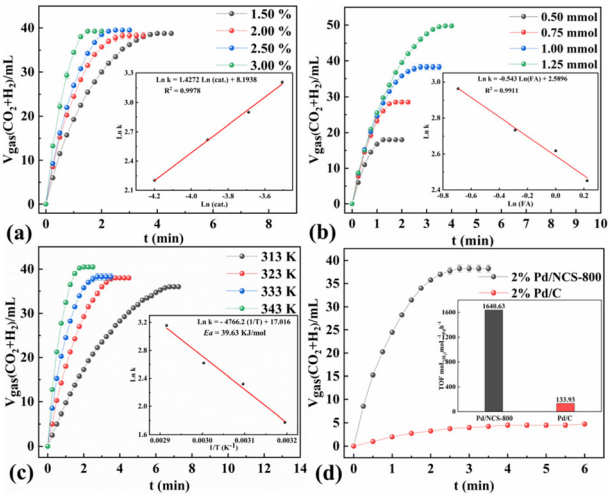

Fig. 6 The volumes of generated CO_2 and H_2 gases *vs.* time for H_2 generation upon additive-free HCOOH dehydrogenation (a) with various amounts of the catalyst, (b) with different amounts of HCOOH and (c) at different reaction temperatures; (d) comparison of additive-free HCOOH dehydrogenation catalyzed by Pd/NCS-800 and Pd/C.

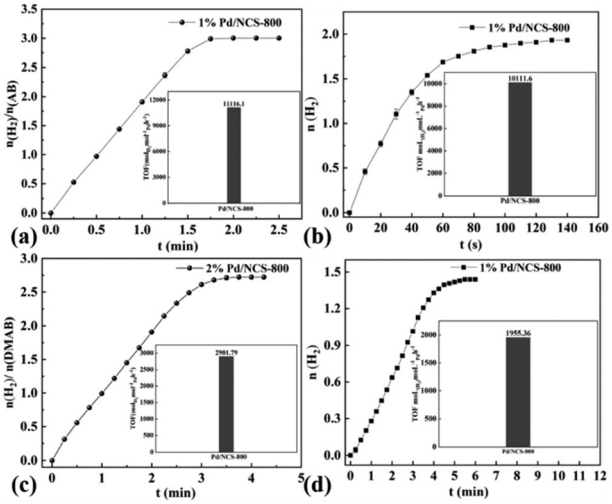

Fig. 7 Pd/NCS-800 catalyzed H_2 generation from (a) ammonia borane, (b) $B_2(OH)_4$, (c) dimethylaminoborane and (d) tetramethyldisiloxane at 30 °C.

catalyst dosage increased, with a slope of 1.4, illustrating that there was a linear positive relationship between them. As presented in Fig. 6b, the H_2 production rate was independent of the initial HCOOH concentration, indicating that additive-free HCOOH dehydrogenation was a zero-order reaction with the initial HCOOH concentration. Then H_2 generation upon additive-free HCOOH dehydrogenation over Pd/NCS-800 was measured at various reaction temperatures from 313 to 343 K (Fig. 6c). The E_a of H_2 generation upon additive-free HCOOH dehydrogenation over Pd/NCS-800 was obtained to be 39.63 kJ mol^{-1}. The comparison of Pd/NCS-800 and commercial Pd/C in H_2 generation upon additive-free HCOOH dehydrogenation was recorded and is shown in Fig. 6d. The result shows that Pd/NCS-800 (1640 h^{-1}) provided a 12 times larger TOF than commercial Pd/C (134 h^{-1}) in H_2 generation upon additive-free HCOOH dehydrogenation. In addition, the Pd/NCS-800 catalyst also showed excellent catalytic performance in H_2 generation from NH_3BH_3 ($NH_3BH_3 + 4H_2O \rightarrow NH_4B(OH)_4 + 3H_2\uparrow$, TOF = 11 116.1 h^{-1}, Fig. 7a), tetrahydroxydiboron ($B_2(OH)_4 + 2H_2O \rightarrow 2B(OH)_3 + H_2\uparrow$, TOF = 10 111.6 h^{-1}, Fig. 7b), dimethylaminoborane ($Me_2NHBH_3 + 4H_2O \rightarrow Me_2NH_2B(OH)_4 + 3H_2\uparrow$, TOF = 2902 h^{-1}, Fig. 7c) and tetramethyldisiloxane ($[Me_2SiH]_2O + 2H_2O \rightarrow [Me_2Si(OH)]_2O + 2H_2\uparrow$, TOF = 1955 h^{-1}, Fig. 7d), confirming that the Pd/NCS-800 catalyst is a versatile and applicable catalyst.

The stability of the Pd/NCS-800 catalyst in H_2 generation upon additive-free HCOOH dehydrogenation was investigated for further industrial application.[56] When H_2 generation was completed, the Pd/NCS-800 nanocatalyst was isolated and recycled by filtration. Next, another fresh HCOOH solution was injected into the medium for next recycling. As described in Fig. S9,† it is clear that the Pd/NCS-800 catalyst still maintained excellent catalytic activity at least for 5 cycles in H_2 generation upon additive-free HCOOH dehydrogenation without any activity loss. Then, the 5 times reused Pd/NCS-800 catalyst was further analyzed by XRD, and Fig. S10† shows that its crystal structure remained almost the same as that of the fresh one, demonstrating that Pd/NCS-800 is a heterogeneous and recyclable nanocatalyst for H_2 generation upon additive-free HCOOH dehydrogenation.

H_2 generation upon additive-free HCOOH dehydrogenation is applied not only for safe and economical production, storage and transportation of hydrogen, but also for a tandem reaction.[57] 1,1-Diphenylethylene hydrogenation with the *in situ* released H_2 from additive-free HCOOH dehydrogenation was carried out in a two-chamber reactor (Scheme 2). The left tube was applied for H_2 generation upon additive-free HCOOH dehydrogenation, and the right one was applied for 1,1-diphenylethylene hydrogenation with the H_2 from the left tube *via* a glass tube (Fig. S11†). The yield of the target product (1,1-

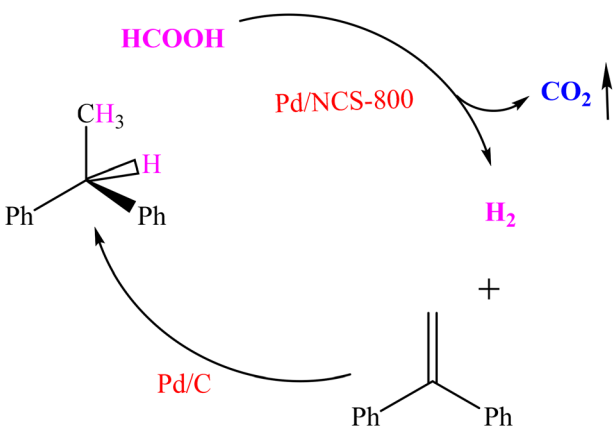

Scheme 2 The tandem reaction.

diphenylethane) was 99% (Fig. S12†), illustrating selective H_2 generation upon additive-free HCOOH dehydrogenation.

For verifying the selective H_2 generation upon additive-free HCOOH dehydrogenation, a gas mixture was passed through a NaOH solution for CO_2 absorption. As shown in Fig. 8a, the volume of the gas mixture was reduced by half with the sodium hydroxide trap, suggesting that the released gases were H_2 and CO_2, with a volumetric ratio of 1.0 : 1.0. Then the released gases were also confirmed by GC to be H_2 and CO_2, with a molar ratio of 1.0 : 1.0 (Fig. 8b). The CO_2 capture test and GC analysis verified that the selective H_2 generation upon additive-free formic acid dehydrogenation over the Pd/NCS-800 catalyst was successfully designed for fuel cells. Based on the CO_2 capture test, GC analysis and relevant literature,[58,59] a possible mechanism involved in HCOOH dehydrogenation is discussed in Fig. S13.† First, a HCOOH molecule was decomposed into Pd–H and HCOO–Pd on the surface of Pd/NCS-800. Then, CO_2* and Pd–H were formed from HCOO–Pd *via* β-hydride elimination. Finally, H_2 was obtained by the reductive elimination of two Pd–H molecules.

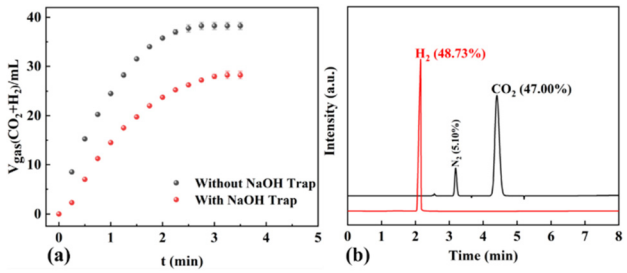

Fig. 8 (a) HCOOH dehydrogenation over Pd/NCS-800 with and without a sodium hydroxide trap; (b) GC spectra of the gases released from additive-free HCOOH dehydrogenation at 60 °C.

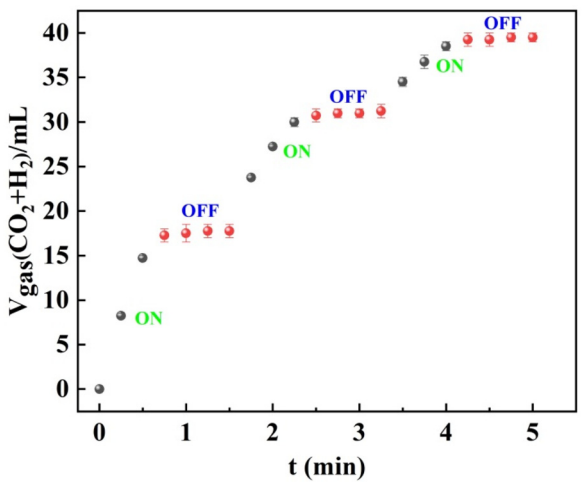

Fig. 9 "On–off" switch of H_2 generation upon additive-free formic acid dehydrogenation. Reaction conditions: 1 mmol of formic acid and 2 mol% of Pd/NCS-800 in water (5 mL) at 60 °C.

The exploitation of the "on–off" switch for demand-based H_2 production is highly desirable.[60–62] As demonstrated in Fig. 9, selective H_2 generation upon additive-free HCOOH dehydrogenation over Pd/NCS-800 was successfully controlled by adjusting the pH. Specifically, H_2 generation upon additive-free HCOOH dehydrogenation stopped after the addition of NaOH solution because formic acid converted into formate. Then, H_2 generation upon additive-free formic acid dehydrogenation restarted after the addition of H_2SO_4 solution due to the regeneration of formic acid. However, a slight decrease in the H_2 generation rate was recorded after each "on–off" switch, which may be caused by the dilution effect.

The catalytic performances of Pd/NCS-800 and other reported catalysts for H_2 generation upon additive-free HCOOH dehydrogenation were compared and are shown in Table S1.†[63–72] The result shows that Pd/NCS-800 exhibited an excellent TOF of 1641 h^{-1}, illustrating that Pd/NCS-800 is an excellent catalyst for selective and controlled H_2 generation upon additive-free HCOOH dehydrogenation.

Conclusions

In summary, a battery of N-doped carbon nanosphere-stabilized Pd nanoparticles (Pd/NCSs) have been synthesized as high-efficiency nano-catalysts, *via* fixation of Pd nanoparticles onto N-doped carbon nanospheres (NCSs), for selective and controlled H_2 generation upon additive-free HCOOH dehydrogenation. The characterization studies confirmed that Pd/NCS-800 has a homogeneous nanospherical structure, and PdNPs are stabilized onto the surface of N-doped carbon nanospheres. Pd/NCS-800 showed superior catalytic performance, with a TOF of 1640 h^{-1}, compared to Pd/NCS-700 (1456 h^{-1}) and Pd/NCS-900 (921 h^{-1}) in H_2 generation upon additive-free HCOOH dehydrogenation. The CO_2 capture test, GC analysis and tandem reaction verified that selective H_2 generation upon additive-free formic acid dehydrogenation over the Pd/NCS-800 catalyst was developed for fuel cells. Pd/NCS-800 (1640 h^{-1}) provided a 12 times larger TOF than commercial Pd/C (134 h^{-1}) in H_2 generation upon additive-free HCOOH dehydrogenation. It seemed that graphitic N/C of NCS-800 enriched the electron cloud density of the Pd atom, which was favorable for the cleavage of C–H bonds in HCOOH dehydrogenation. In addition, the selective H_2 production from additive-free HCOOH dehydrogenation over Pd/NCS-800 is successfully controlled by adjusting the pH. The strategy derived from glucose in this work might generate new ideas for the development of N-doped carbon nanospheres for selective and controlled H_2 generation.

Author contributions

Q. Zhang: investigation and formal analysis. Y. Wang and X. Jin: formal analysis. X. Liu: project administration, supervi-

sion, resources, conceptualization, and writing – original draft, review & editing.

Conflicts of interest

The authors declare no competing financial interest.

Acknowledgements

Financial support from the NSFC (No. 21805166) is gratefully acknowledged and thanks eceshi (**http://www.eceshi.com**) for the ICP test and Yuan Zhou from Shiyanjia Lab (**http://www.shiyanjia.com**) for GC test.

References

1 S. Kar, M. Rauch, G. Leitus, Y. Ben-David and D. Milstein, *Nat. Catal.*, 2021, **4**, 193–201.
2 X. Liu, W. Hou, Y. Huang, H. Zhao, Z. Song and Y. Huang, *Chem. Eng. J.*, 2022, **433**, 133822.
3 S. Xu, H. Zhao, T. Li, J. Liang, S. Lu, G. Chen, S. Gao, A. M. Asiri, Q. Wu and X. Sun, *J. Mater. Chem. A*, 2020, **8**, 19729–19745.
4 C. Peng, T. Li, Y. Zou, C. Xiang, F. Xu, J. Zhang and L. Sun, *Int. J. Hydrogen Energy*, 2021, **46**, 666–675.
5 H. Song, M. Wu, Z. Tang, J. S. Tse, B. Yang and S. Lu, *Angew. Chem., Int. Ed.*, 2021, **60**, 7234–7244.
6 Y. Peng, Y. Zhang, A. Guo, M. Mao, Y. Wang, Y. Long and G. Fan, *Chem. Eng. J.*, 2022, **433**, 133648.
7 H. Liu, Q. Lei, R. Miao, M. Sun, C. Qin, L. Zhang, G. Ye, Y. Yao, B. Huang and Z. Ma, *Adv. Funct. Mater.*, 2022, **32**, 2207408.
8 N. Kang, X. Wei, R. Shen, B. Li, E. G. Cal, S. Moya, L. Salmon, C. Wang, E. Coy, M. Berlande, J.-L. Pozzo and D. Astruc, *Appl. Catal., B*, 2023, **320**, 121957.
9 M. S. İzgi, O. Baytar, Ö. Şahin and H. Ç. Kazıcı, *Int. J. Hydrogen Energy*, 2020, **45**, 34857–34866.
10 H. N. Abdelhamid, *Int. J. Hydrogen Energy*, 2021, **46**, 726–765.
11 (*a*) X. Zou and Y. Zhang, *Chem. Soc. Rev.*, 2015, **44**, 5148–5180; (*b*) L. Zhang, H. Zhao, S. Xu, Q. Liu, T. Li, Y. Luo, S. Gao, X. Shi, A. M. Asiri and X. Sun, *Small Struct.*, 2021, **2**, 2000048; (*c*) J. Chen, L. Zhang, J. Li, X. He, Y. Zheng, S. Sun, X. Fang, D. Zheng, Y. Luo, Y. Wang, J. Zhang, L. Xie, Z. Cai, Y. Sun, A. A. Alshehri, Q. Kong, C. Tang and X. Sun, *J. Mater. Chem. A*, 2023, **11**, 1116–1122; (*d*) Q. Liu, S. Sun, L. Zhang, Y. Luo, Q. Yang, K. Dong, X. Fang, D. Zheng, A. A. Alshehri and X. Sun, *Nano Res.*, 2022, **15**, 8922–8927.
12 T. Hisatomi, J. Kubota and K. Domen, *Chem. Soc. Rev.*, 2014, **43**, 7520–7535.
13 (*a*) C. C. L. McCrory, S. Jung, I. M. Ferrer, S. M. Chatman, J. C. Peters and T. F. Jaramillo, *J. Am. Chem. Soc.*, 2015, **137**, 4347–4357; (*b*) L. Ouyang, X. He, Y. Sun, L. Zhang, D. Zhao, S. Sun, Y. Luo, D. Zheng, A. M. Asiri, Q. Liu, J. Zhao and X. Sun, *Inorg. Chem. Front.*, 2022, **9**, 6602–6607.
14 J. Wang, W. Cui, Q. Liu, Z. Xing, A. M. Asiri and X. Sun, *Adv. Mater.*, 2016, **28**, 215–230.
15 J. Ran, J. Zhang, J. Yu, M. Jaroniec and S. Z. Qiao, *Chem. Soc. Rev.*, 2014, **43**, 7787–7812.
16 Y. Liu, F. Fu, L. Salmon, B. Espuche, S. Moya, M. Berlande, J.-L. Pozzo, J.-R. Hamon and D. Astruc, *ACS Appl. Mater. Interfaces*, 2023, **15**, 23343–23352.
17 N. Gao, D. Han, T. Yang, Q. Meng, X. Wang, C. Liu, J. Ge and W. Xing, *Appl. Catal., B*, 2023, **336**, 122913.
18 X. Sun, Y. Ding, G. Feng, Q. Yao, J. Zhu, J. Xia and Z.-H. Lu, *J. Colloid Interface Sci.*, 2023, **645**, 676–684.
19 Z. Yuan, T. Cao, M. Deng, J. Ma, S. Geng, C. Yang, Y. Ren, M. Yao, F. Liu and X. Wang, *Fuel*, 2023, **346**, 128333.
20 J. Wang, Y. Yu, H. Yu, W. Wang, L.-L. Shen, G.-R. Zhang and D. Mei, *ACS Catal.*, 2023, **13**, 5135–5146.
21 A. Kumar, P. Daw and D. Milstein, *Chem. Rev.*, 2022, **122**, 385–441.
22 J. Hao, J. Liu, D. Wu, M. Chen, Y. Liang, Q. Wang, L. Wang, X.-Z. Fu and J.-L. Luo, *Appl. Catal., B*, 2021, **281**, 119510.
23 L. Lin, Q. Yu, M. Peng, A. Li, S. Yao, S. Tian, X. Liu, A. Li, Z. Jiang, R. Gao, X. Han, Y.-w. Li, X.-d. Wen, W. Zhou and D. Ma, *J. Am. Chem. Soc.*, 2021, **143**, 309–317.
24 Z. Li, X. Tang, Y. Jiang, Y. Wang, M. Zuo, W. Chen, X. Zeng, Y. Sun and L. Lin, *Chem. Commun.*, 2015, **51**, 16320–16323.
25 C. Wang and D. Astruc, *Chem. Soc. Rev.*, 2021, **50**, 3437–3484.
26 C. Wang, Q. Wang, F. Fu and D. Astruc, *Acc. Chem. Res.*, 2020, **53**, 2483–2493.
27 X. Liu, X. Jin, J. Yan, S. Fan, Y. Wang and D. Astruc, *Appl. Catal., B*, 2023, **324**, 122261.
28 S. Guan, Y. Liu, H. Zhang, R. Shen, H. Wen, N. Kang, J. Zhou, B. Liu, Y. Fan, J. Jiang and B. Li, *Adv. Sci.*, 2023, 2300726.
29 J. Cao, W. Huang, Y. Wang, Q. Zhang and X. Liu, *J. Mol. Liq.*, 2023, **369**, 120917.
30 Z. Li and Q. Xu, *Acc. Chem. Res.*, 2017, **50**, 1449–1458.
31 Z. L. Wang, J. M. Yan, Y. Ping, H. L. Wang, W. T. Zheng and Q. Jiang, *Angew. Chem., Int. Ed.*, 2013, **52**, 4406–4409.
32 Y. Liu, J. Zhang, Y. Li, Q. Qian, Z. Li, Y. Zhu and G. Zhang, *Nat. Commun.*, 2020, **11**, 1853.
33 R. Williams, R. S. Crandall and A. Bloom, *Appl. Phys. Lett.*, 2008, **33**, 381–383.
34 Z. Chen, C. A. M. Stein, R. Qu, N. Rockstroh, S. Bartling, J. Weiß, C. Kubis, K. Junge, H. Junge and M. Beller, *ACS Catal.*, 2023, **13**, 4835–4841.
35 M. Karatok, H. T. Ngan, X. Jia, C. R. O'Connor, J. A. Boscoboinik, D. J. Stacchiola, P. Sautet and R. J. Madix, *J. Am. Chem. Soc.*, 2023, **145**, 5114–5124.
36 W.-F. Peng, X. Sun, Y. Ding, P. Liu, Q. Yao and Z.-H. Lu, *ACS Sustainable Chem. Eng.*, 2023, **11**, 1898–1908.
37 L. Yaacoub, I. Dutta, B. Werghi, B. W. J. Chen, J. Zhang, E. A. Hamad, E. P. Ling Ang, E. Pump, A. B. Sedjerari, K.-W. Huang and J.-M. Basset, *ACS Catal.*, 2022, **12**, 14408–14417.

38 Y. Ding, W. Peng, L. Zhang, J. Xia, G. Feng and Z.-H. Lu, *J. Colloid Interface Sci.*, 2023, **630**, 879–887.
39 M. Deng, A. Yang, J. Ma, C. Yang, T. Cao, S. Yang, M. Yao, F. Liu, X. Wang and J. Cao, *ACS Appl. Mater. Interfaces*, 2022, **14**, 18550–18560.
40 Q. Zhang, Q. Mao, Y. Zhou, L. Zou, D. Zhu, Y. Huang, H. Gao, X. Luo, Y. Mao and Z. Liang, *ACS Sustainable Chem. Eng.*, 2022, **10**, 4599–4609.
41 D.-X. Liu, Y.-T. Zhou, Y.-F. Zhu, Z.-Y. Chen, J.-M. Yan and Q. Jiang, *Appl. Catal., B*, 2022, **309**, 121228.
42 D. H. Carrales-Alvarado, C. López-Olmos, A. B. Dongil, A. Kubacka, A. Guerrero-Ruiz and I. Rodríguez-Ramos, *Appl. Catal., B*, 2021, **298**, 120604.
43 S. Prabu and K.-Y. Chiang, *J. Colloid Interface Sci.*, 2021, **604**, 584–595.
44 C. Martin, A. Quintanilla, G. Vega and J. A. Casas, *Appl. Catal., B*, 2022, **317**, 121802.
45 S. Zhong, X. Yang, L. Chen, N. Tsumori, N. Taguchi and Q. Xu, *ACS Appl. Mater. Interfaces*, 2021, **13**, 46749–46755.
46 C. Wan, L. Zhou, S. Xu, B. Jin, X. Ge, X. Qian, L. Xu, F. Chen, X. Zhan, Y. Yang and D.-g. Cheng, *Chem. Eng. J.*, 2022, **429**, 132388.
47 W. Peng, S. Liu, X. Li, G. Feng, J. Xia and Z.-H. Lu, *Chin. Chem. Lett.*, 2022, **33**, 1403–1406.
48 F. Xu and X. Liu, *ACS Catal.*, 2021, **11**, 13913–13920.
49 F. Xu, J. Yan, Y. Wang and X. Liu, *iScience*, 2023, **26**, 106504.
50 Z. Pi, K. Hou, F. Yao, L. He, S. Chen, Y. Fu, X. Li and Q. Yang, *Carbon*, 2022, **196**, 736–748.
51 Y. Qian, S. Jiang, Y. Li, Z. Yi, J. Zhou, J. Tian, N. Lin and Y. Qian, *Angew. Chem., Int. Ed.*, 2019, **58**, 18108–18115.
52 S. Hyok Ri, F. Bi, A. Guan and X. Zhang, *J. Colloid Interface Sci.*, 2021, **586**, 836–846.
53 W. Huang, F. Xu, D.-S. Li, D. Astruc and X. Liu, *Carbon Energy*, 2023, **5**, e269.
54 D. B. Schuepfer, F. Badaczewski, J. M. Guerra-Castro, D. M. Hofmann, C. Heiliger, B. Smarsly and P. J. Klar, *Carbon*, 2020, **161**, 359–372.
55 C. H. Wu, C. Liu, D. Su, H. L. Xin, H.-T. Fang, B. Eren, S. Zhang, C. B. Murray and M. B. Salmeron, *Nat. Catal.*, 2019, **2**, 78–85.
56 Y. Yan, B. Y. Xia, B. Zhao and X. Wang, *J. Mater. Chem. A*, 2016, **4**, 17587–17603.
57 F. Fu, C. Wang, Q. Wang, A. M. Martinez-Villacorta, A. Escobar, H. Chong, X. Wang, S. Moya, L. Salmon, E. Fouquet, J. Ruiz and D. Astruc, *J. Am. Chem. Soc.*, 2018, **140**, 10034–10042.
58 J. S. Yoo, Z.-J. Zhao, J. K. Nørskov and F. Studt, *ACS Catal.*, 2015, **5**, 6579–6586.
59 F.-Z. Song, Q.-L. Zhu, X. Yang, W.-W. Zhan, P. Pachfule, N. Tsumori and Q. Xu, *Adv. Energy Mater.*, 2018, **8**, 1701416.
60 S. Santra, D. Das, N. S. Das and K. K. Nanda, *Chem. Sci.*, 2017, **8**, 2994–3001.
61 C. Wang, J. Tuninetti, Z. Wang, C. Zhang, R. Ciganda, L. Salmon, S. Moya, J. Ruiz and D. Astruc, *J. Am. Chem. Soc.*, 2017, **139**, 11610–11615.
62 S. Santra, D. Das, N. S. Das and K. K. Nanda, *ACS Appl. Energy Mater.*, 2019, **2**, 260–268.
63 A. Bulut, M. Yurderi, Y. Karatas, M. Zahmakiran, H. Kivrak, M. Gulcan and M. Kaya, *Appl. Catal., B*, 2015, **164**, 324–333.
64 Z. Wang, S. Liang, X. Meng, S. Mao, X. Lian and Y. Wang, *Appl. Catal., B*, 2021, **291**, 120140.
65 I. Barlocco, S. Capelli, E. Zanella, X. Chen, J. J. Delgado, A. Roldan, N. Dimitratos and A. Villa, *J. Energy Chem.*, 2021, **52**, 301–309.
66 Y. Gao, E. Hu, G. Yin and Z. Huang, *Fuel*, 2021, **302**, 121142.
67 Y. Karatas, A. Bulut, M. Yurderi, I. E. Ertas, O. Alal, M. Gulcan, M. Celebi, H. Kivrak, M. Kaya and M. Zahmakiran, *Appl. Catal., B*, 2016, **180**, 586–595.
68 Z.-L. Wang, J.-M. Yan, Y.-F. Zhang, Y. Ping, H.-L. Wang and Q. Jiang, *Nanoscale*, 2014, **6**, 3073–3077.
69 X. Zhao, P. Dai, D. Xu, X. Tao, X. Liu and Q. Ge, *J. Energy Chem.*, 2021, **59**, 455–464.
70 Z.-L. Wang, H.-L. Wang, J.-M. Yan, Y. Ping, O. Song-Il, S.-J. Li and Q. Jiang, *Chem. Commun.*, 2014, **50**, 2732–2734.
71 A. Zhang, J. Xia, Q. Yao and Z.-H. Lu, *Appl. Catal., B*, 2022, **309**, 121278.
72 S. Zhang, Y. Qian and W.-S. Ahn, *Chin. J. Catal.*, 2019, **40**, 1704–1712.